Lipid-based Janus nanoparticles for pharmaceutical and cosmetic applications: Kinetics and mechanisms of destabilization with time and temperature

L. Benrabah, K. Kemel, C. Twarog, N. Huang, A. Solgadi, C. Laugel, V. Faivre

Lipid-based Janus nanoparticles for pharmaceutical and cosmetic applications: kinetics and mechanisms of destabilization with time and temperature.

L. Benrabah[1], K. Kemel[2], C. Twarog[1], N. Huang[1], A. Solgadi[3], C. Laugel[2], V. Faivre[1*]

Short statistical summary

Number of words: 6556 including references

Number of figures: 7 (+ 2 in supporting data)

Number of tables: 1

Lipid-based Janus nanoparticles for pharmaceutical and cosmetic applications: kinetics and mechanisms of destabilization with time and temperature.

L. Benrabah[1], K. Kemel[2], C. Twarog[1], N. Huang[1], A. Solgadi[3], C. Laugel[2], V. Faivre[1*]

[1] Institut Galien Paris-Sud, Université Paris-Saclay, Labex LERMIT, 92296 Châtenay-Malabry France ; [2] Lip(Sys)² Chimie Analytique Pharmaceutique, EA7357 Université Paris-Saclay, 92296 Châtenay-Malabry France; [3] Service d'Analyse des Médicaments et Métabolites (SAMM), SFR-UMS IPSIT, Université Paris-Saclay, 92296 Châtenay-Malabry France.

* corresponding author
Tel. + 33 1 46 83 54 65
Fax. + 33 1 46 83 53 12
e-mail: vincent.faivre@universite-paris-saclay.fr

Abstract:

The aim of this paper is to investigate the time and thermal stability of innovative multicompartmental nanoparticles. These particles, having a hydrophilic side and a hydrophobic side, belong to the family of Janus particles and are promising tools to carry active ingredients with opposite solubilities in a unique nanocarrier. The stability of nanoparticles obtained with mainly two types of polyoxylglycerides (Labrafil® M2125 CS and Labrafil® M1944 CS) has been investigated. The suspensions describe a two-step maturation / destabilization process with an Ostwald ripening phase followed by the coalescence of the particles. The effect of lipid composition and temperature on these steps has been investigated in deep as stability with temperature is a critical parameter to consider in order to envisage the development of any formulation for pharmaceutical or cosmetic uses. These nanoparticles were particularly stable at room temperature as their hydrodynamic diameter did not change significantly for 20 months. Contrarily, a strong dependency to temperature appears when storage temperature increases from 25°C to 43°C. Indeed, Labrafil® M1944 CS seemed to undergo a progressive destabilization where a significant increase of particles size is visible from 25°C and phase separation occurred after 4 months at 32°C. At the opposite, Labrafil® M2125 CS remained stable until 36°C and reached a threshold temperature between 32°C and 36°C after which Labrafil® M2125 CS underwent a consequent increase of particles size at the longer time, i.e. after 6 months. Moreover, Labrafil® M2125 CS formulation was stable at least 3 months at 43°C.

Keywords: Janus nanoparticles, stability, Ostwald ripening, coalescence, polyoxylglycerides

1. Introduction

Particles are generally named *Janus* when they have at least 2 distinct sides with different physical and/or chemical properties; for instance, organic/inorganic or hydrophobic/lipophilic as in our study. The term *Janus* comes from Roman mythology, where it is a god with two opposite faces, facing the past and the future. These particles have the particularity to be anisotropic as the properties are different depending on the directions from their center. As observable with cryo-TEM (Fig. 1), we recently developed lipid-based Janus nanoparticles [1,2] having a hydrophobic lipid compartment (composed of vegetable oil derivatives) and a hydrophilic aqueous compartment bounded by a bilayer composed of phospholipids and nonionic polyoxyethylated surfactants. Due to the different compartments, the Janus particles should be used as an original nanocarrier for administration of molecules having opposite solubilities. These molecules can be active ingredients and/or diagnostic agents for theragnosis purpose. Other lipid-based nanodispersions, i.e. liposomes or internally-self-assembled (ISA)somes such as cubosomes or hexosomes, are able to co-encapsulate hydrophilic and hydrophobic compounds [3,4]. However, compared to these well-known systems, the two compartments are less imbricated in the anisotropic particles developed here, allowing notably incorporation of high amount of exogenous hydrophobic material in the lipid part without leakage of the hydrophilic one or particle destabilization [5]. Moreover, these Janus nanoparticles have interesting permeation enhancer properties after cutaneous administration [6].

The aim of the present work is to explore the physical stability with temperature of these Janus nanoparticles. Indeed, stability is a critical parameter to consider in order to envisage the development of such kind of formulation for pharmaceutical or cosmetic uses. This is all the more true that these particles are composed of complex lipid-based excipients.

2. Material and methods

2.1. Material

Gelucire® 50/13 (stearoyl macrogolglycerides; mixture of monoesters, diesters and triesters of glycerol (~20 wt%) and monoesters and diesters of polyethylene glycols (~80 wt%) with mean molecular mass of 1500; mainly contains esters of stearic acid), Labrafil® M 2125 CS (linoleoyl polyoxylglycerides; mixture of monoesters, diesters and triesters of glycerol (>60 wt%) and monoesters and diesters of polyethylene glycols (<40 wt%) with mean molecular mass of 300; mainly contains esters of linoleic acid), and Labrafil® M1944 CS (oleoyl polyoxylglycerides; mixture of monoesters, diesters and triesters of glycerol (>60 wt%) and monoesters and diesters of polyethylene glycols (<40 wt%) with mean molecular mass of 300; mainly contains esters of oleic acid) were given by Gattefosse S.A.S. (Saint-Priest, France). Labrafils are liquid at room temperature while Gelucire® 50/13 is solid. Phospholipon® 90G (soybean lecithin at 94 – 102% of phosphatidylcholine) was provided by Phospholipid GmbH, Lipoid Group (Köln, Germany). Water was purified through a Milli-Q water

system (Millipore, France). Dichloromethane, acetone, acetonitrile HPLC quality were purchased from Sigma-Aldrich (Saint-Quentin Fallavier, France).

2.2. Methods

2.2.1. Preparation of nanodispersions by high-pressure homogenization process

38.5 ml of pre-heated (55°C) aqueous phase containing 1g of stearoyl macrogolglycerides (Gelucire® 50/13) and 0.5g of soybean lecithin (Phospholipon® 90G) as surfactant was formed by using ultra-turrax (IKA® T18, Germany) at 11,000 rpm for 5 min. Thereafter, 10g of lipid phase (Labrafil® M 2125 CS or Labrafil® M1944 CS), heated at 55°C, was added to the water phase and formed a pre-dispersion at 20,000 rpm for 5 min. The resulting dispersion was homogenized at the same temperature by using a two stages high pressure homogenizer (APV2000, Denmark) during 5 min. The homogenization pressures were constantly kept at 600 and 60 bars, in the first and second stages respectively during the whole process. The formulation was collected and cooled down slowly to room temperature (RT) in glass vials. Resulting from a partial phase separation, the formation mechanism of these JNP has been proposed in a previous paper [1]. Briefly, after dispersion and homogenization at high temperature, a multiple emulsion is formed with internal aqueous globules stabilized with alkyl-short PEG derivatives and intermediate oil globules stabilized by lecithin and alkyl-long PEG derivatives; then a water flux and phase separation occurs into the nanodroplets when the hydrophilicity of the PEG-300 esters increases during cooling and the excess of lamellar phase, due to PEG-300 esters, contribute to the bilayer that surround the aqueous compartment.

2.2.2. Particle size measurements

The particle size of nanodispersions were measured using a Nano-ZS90 apparatus (Malvern Instruments, Orsay, France). The average hydrodynamic diameter and polydispersity index (PdI) were determined by dynamic light scattering. The samples were diluted to 1/300 in Milli-Q water before analysis.

2.2.3. Cryogenic transmission electron microscopy (Cryo-TEM)

The morphology of nanodispersions was observed using a cryo-TEM system (JEM 2100, JEOL, Japan). All nanodispersions were diluted to 1/40 (v/v) in Milli-Q water. 10 µl of samples were placed on a copper grid, and the solution excess was carefully removed by a filter paper. The film vitrification was achieved by rapidly plunging the grid into liquid ethane. The vitrified sample was then transferred to the microscope. The temperature was kept about -180°C during both the transfer and the viewing procedure to prevent sample perturbation and the formation of ice crystals.

2.2.4. Physical stability studies with temperature

To compare the hydrodynamic diameter of each formulation, at the same time but with different storage temperature, a laboratory-made plate has been set up in which closed tube series containing 5ml of different formulations have been placed. To maintain a temperature gradient, this plate was cooled at one side using cold water and heated at the other side using a heater. The water and the heater have been set in a way that the minimum temperature would be 25°C and the maximum would be 43°C (Storage temperatures: 25, 28, 32, 36, 39 and 43 ± 0.5°C). All the tube positions were checked regularly using a temperature sensor to know the exact temperature. 5 µl of suspension were taken at defined times during 6 months for size analysis. Size measurement were done at 25°C.

2.2.5. X-ray diffraction (XRD)

X-ray scattering experiments were performed on the 5.2L beamline at ELETTRA Synchrotron Light Laboratory (Trieste, Italy). The energy and wavelength of the incident X-ray beam were 8 KeV and 1.54 Å, respectively. The samples were thermostated in a laboratory-made sample holder, Microcalix, allowing both sample temperature control and simultaneous differential scanning calorimetry analysis. Small-angle (SAXS) and wide-angle (WAXS) X-ray scattering patterns were recorded simultaneously using a 2D single photon counting detector (Pilatus 100K) based on hybrid pixel technology (Dectris, Swiss) and a position-sensitive linear gas detectors filled with an argon-ethane mixture respectively. After 2D-image treatment in the SAXS experiments, the scattered intensity was reported as a function of the scattering vector $q = 4\pi\sin\theta/\lambda = 2\pi/d$, where 2θ is the scattering angle, λ is the wavelength and d is the repeat distance between two reticular plans. The calibration of the WAXS and SAXS detectors were achieved using pure tristearin (2Lβ form), characterized by short spacings of 4.59, 3.85 and 3.70 Å ± 0.01 Å and silver behenate characterized by a long spacing of 58.380 Å ± 0.001 Å, respectively. The samples were loaded into quartz capillaries (Quarzkapillaren, Germany) with external diameter of 1.4 ± 0.1 mm and a wall thickness of 0.01 mm. All data were analyzed with the IGOR Pro software (WaveMetrics, Inc. USA).

2.2.6. Interfacial tension measurements

The interfacial tension measurements were performed using a drop tensiometer (Tracker, Teclis Instrument). The oily solutions (Labrafils) were introduced into a 500 µl syringe with a 180°-curved and hydrophobized needle (gauge N°18). By automated pressure on the piston, the rising drop were formed in the aqueous phase contained in a quartz tank. The measurements were carried out at different temperatures, from 60°C to 25°C, with 5°C-steps, over a period of 15 minutes per temperature after its stabilization. To determine the variation of the interfacial tension of the oil/water interface, each measurement was carried out three times for each temperature and measured densities (section below) were introduced in the calculation sheet.

2.2.7. Density measurements

Interfacial tension measurements need to know the density of liquids as a function of temperature. A vibrating tube densimeter (Anton-Paar, France) was used as an indirect method for measuring the density of the different excipients used in the aqueous phase and oily phase of the Janus particles. The mechanical behavior of the tube in response to the vibration makes it possible to directly calculate the density of the fluid from the oscillation period. The measurements were carried out with increasing temperatures ranging from 20°C to 55°C with 5°C increments. For lipid excipients, the densities obtained at 20°C were in accordance with specifications given by the supplier.

For each product, the evolution of the density with temperature was modeled by a polynomial function of degree three, $D=a+b(T-25)+c(T-25)^2+d(T-25)^3$ where a is the product density at 25°C and b, c and d are characteristic constant of each fluid. These constants were then integrated into the droplet analysis software used for interfacial tension measurements.

2.2.8. LC-MS analysis

HPLC instrumentation was from Thermo Fisher Scientific (Bremen, Germany). Vintage Series KR C18 column (250×4.6 mm, 5 µm) came from Interchim (Montluçon, France) and was thermostated at 25°C. The mobile phase was mixtures of acetonitrile and acetone. More precisely, a mixture acetonitrile/acetone, 97/3 (v/v), was applied in the first ten minutes, then an automatic gradient was applied from 10 min to 100 min until reaching 60/40 (v/v) of acetonitrile/acetone then maintained at 60/40 from 100 to 200 min. The flow rate was set at 1 mL/min with automatic injection of 20 µL. All samples were diluted at 1/100 in a mixture of acetonitrile and dichloromethane 50/50 (v/v). For each Labrafil, two batches were analyzed, with three injections for each batch. In each sample the same standard molecule was added, N-Lauroyl-D-sphingosine at 1mg/mL.

HPLC is coupled with LTQ-Orbitrap velos Pro mass spectrometer from Thermo Fisher Scientific (Bremen, Germany). The signal was acquired with Xcalibur software from Thermo Fisher Scientific. The spectrometer was a hybrid device incorporating two analyzers, a double linear ion trap (at high and low pressure) and a Fourier Transform orbital trap. The ionization source used was atmospheric pressure photoionization (APPI), using the positive-ion mode. Vaporizer temperature of the probe was set at 350 °C. Sheath gas, auxiliary gas, and sweep gas flow rates were set at 40, 20, and 0 (arbitrary unit) respectively. Capillary temperature was set at 325 °C and S-lens RF level at 60%. The data was acquired in the mass range m/z 150.00-1100 and analyzed with MZmine 2 [7].

3. Theoretical background

Because they are not usual, there are no studies on the stability of the nanoparticles developed in the present paper. Based on comparison with classical lipid dispersions as emulsions, the potential destabilization mechanisms have been summarized in the following sections. The Janus nanoparticles require important energy input to be formed (high pressure homogenization), confirming they are thermodynamically unfavorable systems that tend to evolve with time.

206
207 Gravitation vs Brownian motions
208
209 Dispersed droplets are theoretically moved by two forces in the continuous medium: Brownian and
210 gravitational forces. Gravitational forces induce the upward movement of the emulsion droplets which
211 have a lower density than the surrounding liquid while a downward movement is obtained when the
212 droplets have a higher density. These phenomena, corresponding to creaming and sedimentation
213 respectively, are the most common processes of apparent destabilization.
214
215 The velocity of a particle submitted to gravitational forces is given by Stokes law (Eq. 1):
216
217 $$v_{Stokes} = \frac{g d^2 (\rho_d - \rho_c)}{18 \eta_c}$$
218
219 where v_{stokes} is the droplet Stokes velocity, g is the gravity acceleration, d is the diameter of the
220 particle, ρ_d is the droplet density, ρ_c is the continuous phase density and η_c is the continuous phase
221 shear viscosity.
222
223 In dilute dispersion, small particles / droplets display erratic motions named Brownian motions. They
224 are due to heat motion of the continuous phase molecules which collide with the particles. A basic
225 relation in this field is the Stokes-Einstein equation which links the macroscopic diffusion coefficient
226 D to the properties of the system (Eq. 2):
227
228 $$D = \frac{k_B T}{6 \pi \eta_c r}$$
229
230 Where k_B is the Boltzmann constant, T is the temperature and r is radius of the particle.
231
232 It is apparent from equations (1) and (2) that the size of the dispersed entities is a key-parameter
233 affecting their motion with time. Indeed, compared to larger ones, small sizes will decrease the motion
234 velocity induced by gravitational forces and increase the random Brownian motion. Thus, it is
235 generally admitted that for nanoemulsions having droplet diameter around 100-200 nm, the gravitation
236 can be entirely neglected in comparison with the Brownian force. It means that such nanodispersions
237 are not sensitive to creaming (or sedimentation). It should be all the more true with the Janus
238 nanoparticles. Indeed, in addition to their small sizes, their density will reduce their Stokes velocity.
239 The lipophilic compartment will have a density like oil (~0.9) [8] while the aqueous compartment
240 could be assimilated to liposomes which have density slightly higher than one (~1.05) [9]. Their

combination will give a density of the Janus nanoparticles close to 1, reducing thus the density gradient with the continuous phase and then the gravitation effect. To summarize, Brownian motion should keep the Janus nanoparticles almost evenly distributed throughout the dispersion.

Destabilization mechanisms

Mainly four mechanisms can lead to nanoemulsion destabilization: flocculation, coalescence, Ostwald ripening and creaming. Flocculation refers to reversible aggregation of the droplets without any change in primary droplet size while coalescence implies the fusion of two or more droplets into larger ones by disruption of the liquid film between the droplets. Ostwald ripening corresponds to the dissolution of the smallest droplets into larger droplets [10]. With time, all these mechanisms result in a droplet size distribution shifts to larger values than can lead to creaming and total phase separation in the worse cases.

In the present work, the physical stability of the Janus nanoparticle dispersion will be followed by hydrodynamic diameter measurements after gentle agitation. Ostwald ripening and coalescence are the two mechanisms that can lead to size increase.

Among polydisperse population, Ostwald ripening results to the growth of large droplets at the expense of smaller ones thank to the diffusion of lipid phase molecules through the continuous phase. The droplet growth rate is often interpreted with the diffusion-controlled model described in the well-known Lifshitz-Slyozov and Wagner theory (Eq. 3) [11,12]:

$$d_t^3 - d_0^3 = \frac{64\gamma D_m V_m C_\infty}{9RT} t = \omega_o t$$

Where d_0 is the initial diameter, d_t is the average droplet diameter at time t, γ is the interfacial tension, D_m is the molecular diffusion coefficient of the dispersed phase, V_m is the molar volume of the oil, C_∞ is the solubility of the dispersed phase into the continuous phase and R is the gas constant. This equation indicates that the cube of the mean droplet diameter should increase linearly with time for emulsion undergoing Ostwald ripening with the rate ω_o.

On the other hand, coalescence could be modelled by the following law (Eq. 4) [13]:

$$\frac{1}{d_0^2} - \frac{1}{d^2} = \frac{2\pi}{3} \omega_c t$$

Where ω_c is the coalescence rate.

4. Results

4.1. Preliminary results

In a previous paper [1], the physical stability of the Janus dispersion has been monitored by following the hydrodynamic diameter of three different batches during 14 months. The size has not changed significantly during this period of storage in closed glass vials kept in a thermostated room (21 ± 0.5°C) and in the dark. During the same time lapse, polydispersity indexes (the square of the standard deviation divided by the square of the mean) were stable around 0.1 suggesting narrow size distributions. This study was continued to reach more than 2 years. This update is described in Figure 2. Several modifications were observed during this extended period. On the one hand, the hydrodynamic diameter seemed to increase very slowly during 20 months while it increased suddenly at 28 months. On the other hand, the polydispersity of the suspension decreased after 20 months and then tends to grow-up at 28 months. These profiles strongly suggested that two processes occurred within the dispersion during the longtime storage. More precisely, Ostwald ripening mechanism is perfectly coherent with the slight size increase and the simultaneous polydispersity index decrease while the late raise could be the beginnings of coalescence.

To confirm such results and to deeply investigate the impact of storage temperature, new stability studies were done. The duration and the temperature ranged were fixed at 6 months and between 22°C to 43°C, respectively to cover stability study conditions (40°C) widely spread in the cosmetic and pharmaceutical fields. Two polyoxylglycerides mixtures (Labrafil® M2125CS and M1944CS) were compared.

4.2. Stability studies between 22°C to 43°C

As the previous studies tend to show that the formulations of interest remain stable at controlled room temperature (21°C) and at 4°C (data not shown), the behavior of the dispersions was studied at higher temperatures.

Basic formulations with either Labrafil 1944CS® (L1944) or Labrafil 2125CS® (L2125) were stored in a temperature-controlled plate and their particles average size and PdI measured each week during 28 days and then every month during 6 months. Figure 3 summarize the results. It appeared that the two Labrafils had very different behaviors under these conditions. Indeed, between 25°C and 43°C, L1944 seemed to undergo a progressive destabilization (Fig. 3A) where a significant increase of particles size is visible from 25°C and phase separation occurred after 4 months at 32°C. At the opposite, L2125 remained stable until 36°C and reached a threshold temperature between 32°C and 36°C after which L2125 underwent a consequent increase of particles size at the longer time, i.e. after 6 months. Moreover, L2125 formulation was stable at least 3 months at 43°C (Fig. 3B). To

summarize, the increase underwent by L2125 was less than that of L1944 along the temperature and the time.

In order to investigate a possible concentration effect on the particle stability, similar experiments were done with 1-to-1 water diluted suspensions where the labrafil concentrations decreased from 20% (w/w) to 10%. Same trends were observed in term of stability but with an interesting shift towards higher temperature (Figs. 3C-D). Thus diluted L2125 formulation is totally stable during 6 months at 36°C and phase separation occurred only after 5 months at 39°C. Diluted L1944 formulation is still progressively destabilized with time even at relatively low temperature (at 28°C after 6 months) but it was stable 5 months at 36°C while the concentrated one is totally destabilized (phase separation) after 4 months at this temperature.

4.3. Density measurements

Densities with temperature of both Labrafils are described in Figure 4A. They evolved linearly with temperature between 55°C and 20°C, from 0.920 to 0.945 for L2125 and from 0.917 to 0.942 for L1944. These values were similar to supplier data and were not very different between the two Labrafils.

4.4. Surface tension measurements

Labrafils are oily excipients composed of a glycerides and PEG esters. These esters are non-ionic surfactant with polyethoxylated short chains and are known to have different affinity for lipid and aqueous compartments depending on the temperature. This is due of the progressive dehydration of the PEG chains leading to an increase of hydrophobicity with increasing temperature. This phenomenon is related to the work of Shinoda and al who have stated that there is a Phase Inversion Temperature (PIT) at which this kind of surfactants become more hydrophobic or more hydrophilic [14]. As the Labrafils contain these non-ionic surfactants, it has been proposed to investigate surface tension of the oil droplets. Indeed, surface tension of the oil is directly depending on the surfactant properties and could be used to determine the PIT of lipid mixtures as the surface tension reach a minimum at this critical temperature. Figure 4B summarizes the surface tension measurements obtained with both Labrafil between 55°C to 25°C. As expected, surface tension decreased with decreasing temperature to reach a plateau for L2125 and a minimum for L1944 at around 39°C. For the later, surface tension slightly increased at lower temperature. As the PEG esters amount is important, surface tension values are low.

4.5. X-ray diffraction experiments

X-ray diffraction experiments have been done on both Labrafils, containing or not water and at different temperature, in order to extend their comparison. With pure excipients, no diffraction peaks were visible both at 20°C and 60°C (data not shown). The SAXS pattern only suggested the presence

of diffusing objects into this complex excipient, certainly inverse micelles of the polyoxyethylene alkyl derivatives into the glycerides. The addition of small amounts of water into Labrafil excipients, here 10 wt%, led to the growth of two diffraction peaks characterizing a lamellar organization at 20°C, with a period of 87 Å and 96 Å for L2125 and L1944, respectively (Figure 5A-B). The organizations we observed are sensitive to temperature as they totally disappeared above ~38°C and ~31°C for L2125 and L1944, respectively. This lamellar organization is consistent with previous work from Kunieda and co-workers [15] who investigated the phase behaviour of poly(oxyethylene) unsaturated-C18 ether in water at room temperature. Surfactants having mean chains of 6 EO (PEG300) generates lamellar phases on a large extend of hydration, from less than 10 wt% of water to fully hydrated phases with excess water. The different period observed here could be explained by the nature of the main alkyl chains constituting the Labrafils, notably the number of double bonds. Indeed, Fidalgo-Rodriguez et al [16] have shown, with monolayer experiments at the air-water interface, that self-organized oleic acid-based monolayer are thicker than linoleic acid based monolayer due to the torsion and tilt angles imposed by the supplementary unsaturation. At higher temperature, a signal of diffusion was maintained for both Labrafils suggesting the incorporation of water droplets into the alkyl polyoxylglycerides. The presence of this water-in-oil dispersion seems consistent with an increase of the packing parameter of the polyoxyethylene alkyl derivatives with temperature thanks to the dehydration of the polar head allowing the transition from a lamellar organization to an inverted structure.

4.6 Composition comparison

The composition of L2125 and L1944 was investigated carefully by LC-MS analysis. The methodology and the full results will be published soon (accepted manuscript, [17]) but the key-points for the present stability study are summarized in Table 1. More precisely, *m/z* intensity ratio of L2125 and L1944 ($\frac{I_{m/z(2125)}}{I_{(m/z(1944)}}$) was calculated for more than 40 compounds identified in these excipients and values above 2 or below 0.5 were considered. Indeed, a value higher than 2 indicated that the proportion of the compound of interest was significantly higher in L2125 compared to L1944 while a value lower than 0.5 corresponded to the reverse situation. It appeared from this analysis than the proportion of five triglycerides (OOO, OOS, LLL, LLP and LPP), four diglycerides (1,3-OO , 1,2-OO, 1,3 LL and 1,3-LL) and homogeneous di-esters of PEG (O-PEG$_n$-O and L-PEG$_n$-L) were significantly different between the two excipients. In contrary, these mixtures did not differ a lot regarding PEG-monoesters, heterogenous PEG-diesters (two different fatty acids) and other glycerides (mono-, di- and triglycerides). To complete this overview, it is important to mention that the median of the PEG chain distribution in the PEG-esters is in the range $5<n<6$.

5. Discussion

Raw analysis of the stability data strongly suggested a better stability of the L2125 systems compared to L1944 and a better stability of the diluted systems compared to the concentrated ones. Some calculations using the models described in the theoretical background section have been used to elucidate the destabilization mechanisms of these Janus nanoparticles. For most of the conditions (composition of the dispersion and storage temperature), the data treatment by equations (3) and (4) allowed to clearly distinguish two regimens during the stability studies. An example is given in Figure 6 where the size results of non-diluted L1944 particles stored at 28°C were expressed as d^3 or $1/d^2$ and followed with time. It appeared very clearly that d^3 increased slowly and linearly during the first weeks and more rapidly after a certain time of storage; the inflexion point is around 35 days in that case. Symmetrically, $1/d^2$ decreased slowly during the first weeks and then more abruptly. Interestingly, this inflexion point strongly depends on the storage temperature, the type of Labrafil and the Janus particles concentration.

Regarding the evolution of this inflexion point, the two non-diluted dispersions have the same profiles in which the second regimen (rapid increase of d^3 or decrease of $1/d^2$ with time) is immediately observed at high temperature, above 32°C with L1944 and above 39°C with L2125 (supporting information, Fig. S1). At lower temperature, the time for regimen change increased with decreasing temperature and it appeared lately with L2125 compared to L1944. At 21°C, the second regimen appeared only after 150 days of storage for L1944 while the first regime was maintained during the whole study, 180 days, with L2125. Variations are smoother with diluted suspensions in which the first regime was partially kept even at high temperature, until ~30 days and 90 days at 43°C for L1944 and L2125, respectively. These durations increased slowly with decreasing temperature. Interestingly, the first regime was maintained during the 180 days of the study for diluted L2125 suspensions stored at 36°C or below.

The first regime was compared at 28°C because this temperature allowed to compare the different formulations with enough data, at least five points per condition (supporting information, Fig. S2). Because of the withdraw of the size distribution, the mean size did not change significantly and the Ostwald ripening rate, ω_o, was not significantly different from 0 for diluted L2125 formulation while it was 1.0 $x10^4$ nm^3/day, 1.1 $x10^5$ nm^3/day and 1.5 $x10^4$ nm^3/day for non-diluted L2125, non-diluted L1944 and diluted L1944 respectively. These values are similar to values reported in the literature for SDS- or Brij 30- stabilized nanoemulsions [18, 19].

Interestingly, to illustrate the temperature dependency, ω_o for non-diluted L1944 jumped to 3 $x10^5$ nm^3/day at 32°C and decreased to 3.1 $x10^3$ nm^3/day at 25°C. For the same Janus suspensions, at the same storage temperature, the coalescence rate, ω_c, corresponding to the second regime, was 4.1 $x10^{-8}$ nm^{-2}/day at 25°C, 3.3 $x10^{-8}$ nm^{-2}/day at 28°C and 4.2 $x10^{-8}$ nm^{-2}/day at 32°C. The same comparison was done with non-diluted L2125 on a larger temperature scale as these Janus nanoparticles were more stable. Thus, ω_o varied from 5.8 $x10^2$ nm^3/day at 25°C to 4.6 $x10^4$ nm^3/day at 36°C and ω_c from 2.0 $x10^{-7}$ nm^{-2}/day at 25°C to 7.2 $x10^{-8}$ nm^{-2}/day at 36°C. It must be observed here that for both Labrafils,

in the investigated temperature ranges, the Ostwald ripening rate increased by 100 times while the coalescence rate changed by less than 3 times.

All these data suggested *i*-that the coalescence rate is not strongly influenced by the temperature, *ii*-the Ostwald ripening rate significantly increased with temperature (more than 10 times per °C), *iii*-the Ostwald ripening rate decreased with dilution, *iv*-the global stability of the suspensions was directly correlated to duration of the ripening phase and *v*-the L2125 Janus nanoparticles are more stable than L1944 nanoparticles.

L2125 Janus nanoparticles and L1944 nanoparticles had significantly different behaviors (similar trends have been observed with other batches of particles (data not shown), notably an Ostwald ripening rate, ω_o, ~10 times lower for the former particles, that must be discussed here. The initial diameter of the dispersion was different as it was 161 nm for L2125 nanoparticles and 226 nm for L1944 nanoparticles. However, it has been shown [20] that the driving force for Ostwald ripening decreases drastically with increasing droplet size, meaning in our case that L2125 nanoparticles should evolved more rapidly than L1944 nanoparticles. Opposite effect has been observed here.

Composition is the second important difference between the two types of nanoparticles. Labrafil® M2125CS, resulting from the partial hydrolysis and esterification of corn oil, contains mainly linoleyl-based structures while M1944CS, coming from apricot kernel oil, is rich on oleyl-based compounds. Among the tens of compounds constituting these excipients, and as expected regarding the fatty acid distribution furnished by the supplier, LC-MS investigations have shown that they differed more significantly by some triglycerides (OOO and SOO in L1944 vs. LLL, LLP and LPP in L2125), diglycerides (OO in L1944 vs. LL in L2125) and their polyethoxylated structures (dioleyl-PEG in L1944 vs. dilinoleyl-PEG in L2125). The PEG-chain lengths varied from 3 to 12 with a median around 6. As described in Eq. 3, ω_o depends on γ , the interfacial tension, D_m, the molecular diffusion coefficient of the dispersed phase through the external phase, V_m, the molar volume of the oil, and C_∞, the solubility of the dispersed phase into the continuous phase. In the investigated temperature range, the interfacial tension values were not very different between the two Labrafils (Figure 4B). The molar volume of the di-unsaturated species (L2125) would be slightly lower compared to mono-unsaturated species (L1944) what could induce a higher ripening rate (Eq. 3). For example, data from literature [21] allowed to calculate a molar volume of 970.4 cm^3/mol for OOO and 949.2 cm^3/mol for LLL at 20°C. These values increase to 984.8 cm^3/mol and 963.2 cm^3/mol respectively at 40°C. However, the extend of variations of the molar volume could not explain the important changes of ω_o observed in the present work. In contrary, D_m and C_∞ should be different between L2125 and L1944. Indeed, it was proposed that micelles possibly play a role in Ostwald ripening by improving mass transfer between lipid droplets. The proposed mechanism is the solubilization of the glycerides into the micelles which lead to an apparent increase of the dispersed phase solubility and improve the molecular diffusion thanks to the inherent dynamic of the micelles. It seemed reasonable to assume

459 that such parameters will depend on the number of micelles in the suspensions. Because of the
460 important amount of surfactants in our suspensions, the presence of micelles is highly probable and
461 will depend on the critical micellar concentrations (CMC) of the constituting molecules. Interestingly,
462 the presence of unsaturation in the hydrophobic chain of the surfactants will increase the CMC as
463 much as factor as 3-4 per double bond [22]. This should lead here to a higher CMC for PEG-esters
464 from L2125 and, consequently, less micelles into the dispersed phase and a lower Ostwald ripening
465 compared to M1944. Furthermore, micelles of ethoxylated surfactants are very sensitive to
466 temperature. To summarize, the CMC clearly decrease with increasing temperature, as the solubility of
467 the polar head group decrease, and the hydrodynamic diameter of the micelles grow with temperature
468 [23]. This would contribute to the significant increase of ω_o observed with temperature in our work for
469 both Labrafils. The proposed micelle-based mechanism is also convenient with the longer Ostwald
470 ripening phase, and then the better stability, observed for the diluted suspensions in which the number
471 of micelles will be lower compared to non-diluted systems.
472 Cryo-TEM experiments were done to check the morphology of some samples after 5 months of
473 storage. Figure 7A, B and C allowed to compare diluted L1944 stored at 21°C (Fig. 7A) and 36°C
474 (Fig. 7B and C). In these conditions, the sample is still in the Ostwald ripening regime at low
475 temperature and in the coalescence regime since ~80 days at the highest temperature. It appeared on
476 these micrographs that Janus particles were undoubtedly present at 21°C while the two compartments
477 were totally separate at 36°C, certainly due to the modification of solubility and packing parameter of
478 the ethoxylated surfactants, which will result with time to the coalescence of the droplets. Some
479 coalescence phenomena seemed observable at 36°C on Figure 7C. Probably because of the cryo-TEM
480 principle that selects smallest particles, largest droplets were not observable.
481
482 **6. Conclusion**
483 The investigations made during that work allowed to identify a two-regimen destabilization
484 mechanism for the Janus nanoparticles. First, a slight size increase by Ostwald ripening and then a
485 rapid coalescence. These phenomena are strongly dependent on temperature of storage. It appeared
486 also that the most efficient way to improve the stability should be to slow down the Ostwald ripening
487 by modifying the composition and the concentration of the formulation. Further works must be done to
488 improve the most stable formulation, diluted L2125, to reach a stability of 6 months at 40°C which is a
489 standard in the pharmaceutical and cosmetic fields. More precisely, Ostwald ripening can be limited in
490 classical emulsion by adding an insoluble oil. In the present case, similar strategy has to be
491 investigated with care as it could interfere with the Janus particle preparation process.
492
493 **Acknowledgment**
494 The authors would like to thank T. Truong Cong, L.T.C Tran and E. Lafon who participated to
495 stability studies. H. Amenitsch contributed to Elettra SAXS measurements and G. Frebourg (UPMC)

to cryo-TEM observations. This project received financial supports from the program “Investissements d’Avenir” (ANR-LABEX).

References

[1] T. Truong-Cong, E. Millart, C.T.L. Le Tuyet, H. Amenitsch, G. Frebourg, S. Lesieur, V. Faivre, Scalable Process to produce Lipid-based Compartmented Janus nanoparticles with pharmaceutically approved excipients. Nanoscale, 10 (2018), pp. 3654 – 3662

[2] V. Faivre, S. Lesieur, M. Ollivon, M. Ouattara, T. Truong-Cong, Multicompartmented lipid nanoparticles. Patent US-9 757 337 (2017)

[3] A.G. Gomez, S. Syed, K. Marshall, Z. Hosseinidoust. Liposomal nanovesicles for efficient encapsulation of Staphylococcal antibiotics. ACS Omega, 4 (2019), pp. 10866-10876

[4] M. Rakotoarisoa, B. Angelov, S. Espinoza, K. Khakurel, T. Bizien, A. Angelova. Cubic liquid crystalline nanostructures involving catalase and curcumin: BioSAXS study and catalase peroxidatic function after cubosomal nanoparticle treatment of differentiated SH-SY5Y cells. Molecules, 24 (2019), 3058.

[5] E. Millart, S. Lesieur S., V. Faivre. Superparamagnetic lipid-based hybrid nanosystems for drug delivery. Expert Opinion in Drug Delivery, 15 (2018), pp. 532-540.

[6] K. Kemel, A. Deniset-Besseau, A. Baillet-Guffroy, V. Faivre, A. Dazzi, C. Lauge.l Nanoscale investigation of human skin and study of skin penetration of Janus nanoparticles. International Journal of Pharmaceutics, 579 (2020), 119193.

[7] T. Pluskal, S. Castillo, A. Villar-Briones, M. Orešič, MZmine 2: Modular framework for processing, visualizing, and analyzing mass spectrometry-based molecular profile data. BMC Bioinformatics 11 (2010), 395

[8] Gattefossé. Technical document Labrafils (2012).

[9] J.R. Philippot, F. Schuber, P. Couvreur, J. Delattre, Les liposomes : aspects technologiques, biologiques et pharmaceutiques. INSERM-EM Inter (1993).

[10] F.T. Tadros, Emulsion Formation and Stability. Wiley-VCH Verlag GmbH (2013).

[11] J. Weiss, N. Herrmann, D.J. McClements, Ostwald ripening of hydrocarbon emulsion droplets in surfactant solutions. Langmuir, 15 (1999), pp. 6652-6657

[12] V. Schmitt, C. Cattelet, F. Leal-Calderon, Coarsening of alkane-in-water emulsions stabilized by nonionic poly(oxyethylene) surfactants: the role of molecular permeation and coalescence. Langmuir, 20 (2004), pp. 46-52

[13] J. Santos, N. Calero, L.A. Trujillo-Cayado, M.C. Garcia, J. Munoz, Assessing differences between Ostwald ripening and coalescence by rheology, laser diffraction and multiple light scattering. Coll. Surf. B., 159 (2017), pp. 405-411

[14] K. Shinoda, H. Arai, The correlation between phase inversion temperature in emulsion and cloud point in solution of nonionic emulsifier. J. Phys. Chem., 68 (1964), pp. 3485-3490

[15] H. Kunieda, K. Shigeta, K. Ozawa, Self-organizing structures in poly(oxyethylene) oleyl ether – water systems. J. Phys. Chem. B., 101 (1997), pp. 7952-7957

[16] J.L. Fidalgo Rodriguez, P. Dynarowicz-Latka, J. Minones Conde, Structure of unsaturated fatty acids in 2D system. Coll. Surf. B., 158 (2017), pp. 634-642

[17] K. Kemel,, S. Tfaili, A. Baillet-Guffroy, A. Solgadi, D. Libong, C. Laugel, Analysis of linoleoyl and oleoyl macrogolglycerides by high performance liquid chromatography coupled to the atmospheric pressure photoionization mass spectrometry, OCL, Accepted manuscript (2020).

[18] T.J. Wooter, M. Golding, P. Sanguansri, Impact of oil type on nanoemulsion formation and Ostwald ripening stability. Langmuir, 24 (2008), pp. 12758-12765

[19] J. Rao, D.J. McClements, Stabilization of phase inversion temperature nanoemulsions by surfactant displacement. J. Agric. Food. Chem., 58 (2010), pp. 7059-7066

[20] F.T. Tadros, Nanodispersions. Degruyter Eds (2016).

[21] T.H. Gouw, J.C. Vlugter, Physical properties of triglycerides. I. Density and refractive index. Eur. J of Lipid Sci., 68 (1966), pp. 544-549

[22] D. Myers, Surfactant science and technology, 3rd Ed. John Wiley and Sons, Inc (2006).

570 [23] K. Holmberg, B. Jonsson, B. Kronberg, B. Lindman, Surfactants and polymers in aqueous
571 solution, 2nd Ed. John Wiley and Sons, Inc (2003).
572

Table

Table 1: *m/z* intensity ratio (L2125 to L1944) summarizing the most important differences between the two Labrafils® in term of composition. O: Oleic (18:1), L: Linoleic (18:2), P: Palmitic (16:0), S: Stearic (18:0). The number of ethylene oxide groups, n, varies from 3 to 11.

Compound	*m/z* intensity ratio (L2125 to L1944)
OOO	0.22
OOS	0.22
LLL	6.5
LLP	7.8
LPP	8.2
1,3-OO	0.37
1,2-OO	0.44
1,3 LL	3.2
1,2-LL	3.5
O-PEG$_n$-O	0.24 ± 0.03*
L-PEG$_n$-L	4.3 ± 0.8*

* Standard deviations here come from the distribution of the ethylene oxide chain length.

Figure captions

Figure 1: Cryo-TEM micrograph of the Janus nanoparticles

Figure 2: Preliminary stability study at 21 ± 0.5°C in the dark of Janus nanoparticles made with Labrafil® M2125CS (20% of Labrafil in the formulation). n=3, meaning three different batches (mean ± SD).

Figure 3: Sum-up of the stability studies. Only one batch per composition and one sample per temperature. Results are expressed as the mean hydrodynamic diameter ± the withdraw of the distribution. Dotted lines correspond to time periods where phase separations were observed for the specified temperatures.

Figure 4: Density (A) and surface tension (B) of the different Labrafils with temperature.

Figure 5: SAXS measurements with temperature of hydrated Labrafil® M2125CS (A) and M1944CS (B). Heating rate: 2°C/min

Figure 6: Size analysis of non-diluted L1944 particles stored at 28°C treated by equations (3) and (4).

Figure 7: Cryo-TEM micrographs of diluted L1944 stored 5 months at 21°C (A) and 36°C (B and C). Scale bar is 200 nm.

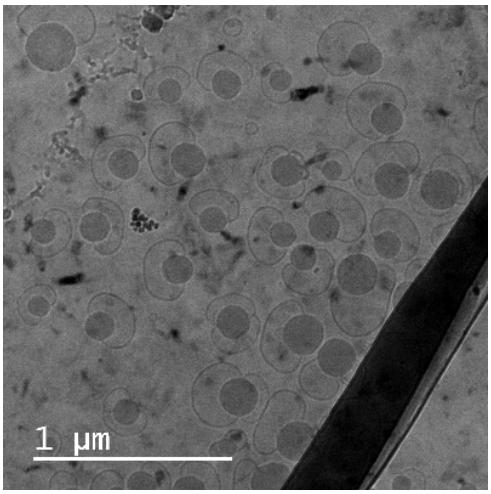

Figure 1

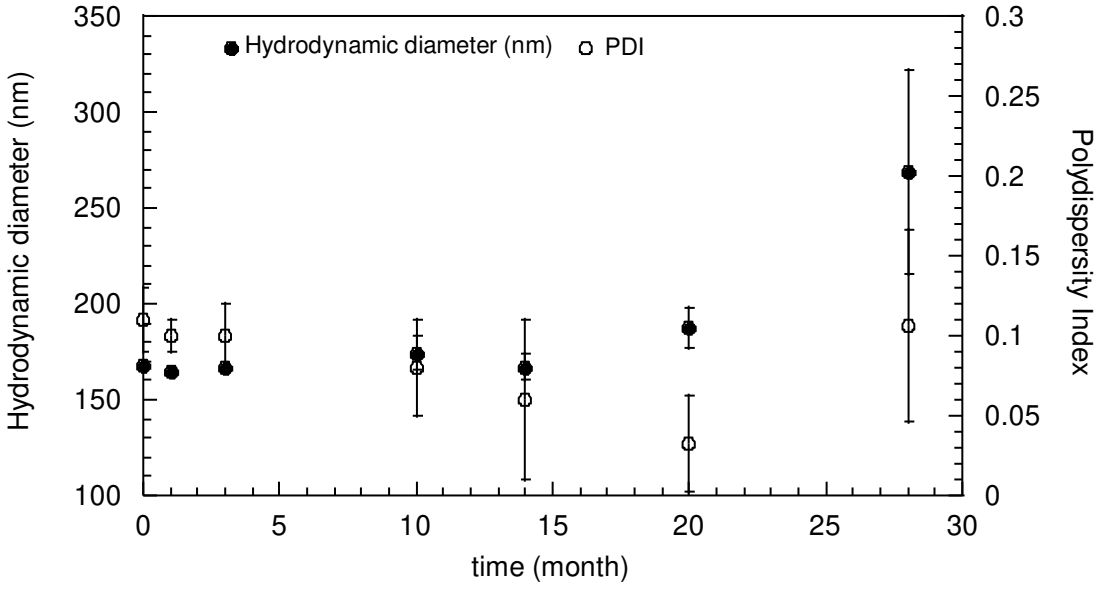
Hydrodynamic diameter (nm)
PDI
Hydrodynamic diameter (nm)
Polydispersity Index
time (month)
350
300
250
200
150
100
0.3
0.25
0.2
0.15
0.1
0.05
0
0
5
10
15
20
25
30

Figure 2

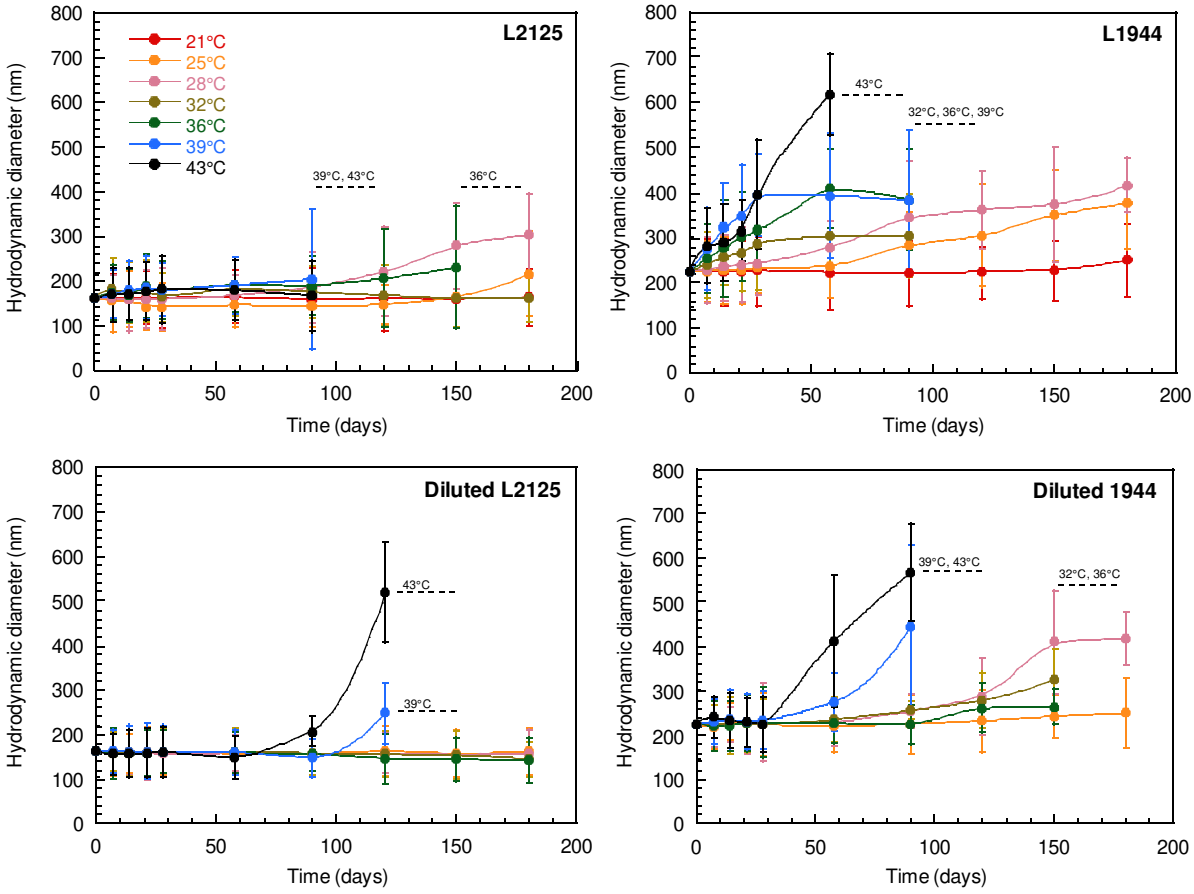
L2125
21°C
25°C
28°C
32°C
36°C
39°C
43°C
39°C, 43°C
36°C
Hydrodynamic diameter (nm)
Time (days)
L1944
43°C
32°C, 36°C, 39°C
Diluted L2125
43°C
39°C
Diluted 1944
39°C, 43°C
32°C, 36°C

Figure 3

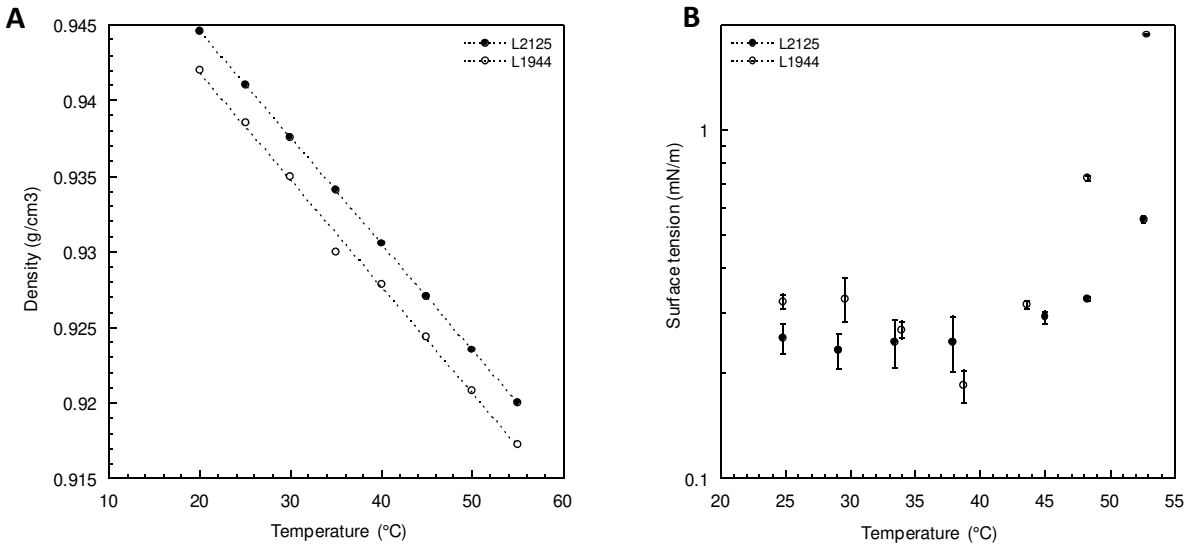
A
0.945
0.94
0.935
0.93
0.925
0.92
0.915
Density (g/cm3)
10
20
30
40
50
60
Temperature (°C)
L2125
L1944
B
1
0.1
Surface tension (mN/m)
20
25
30
35
40
45
50
55
Temperature (°C)
L2125
L1944

Figure 4

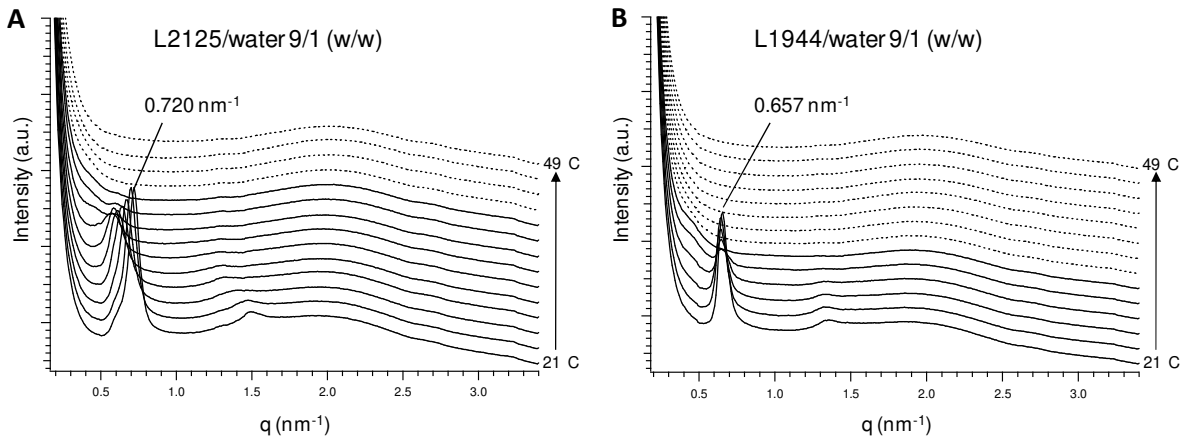
A
L2125/water 9/1 (w/w)
0.720 nm-1
Intensity (a.u.)
49 C
21 C
0.5
1.0
1.5
2.0
2.5
3.0
q (nm-1)
B
L1944/water 9/1 (w/w)
0.657 nm-1
Intensity (a.u.)
49 C
21 C
0.5
1.0
1.5
2.0
2.5
3.0
q (nm-1)

Figure 5

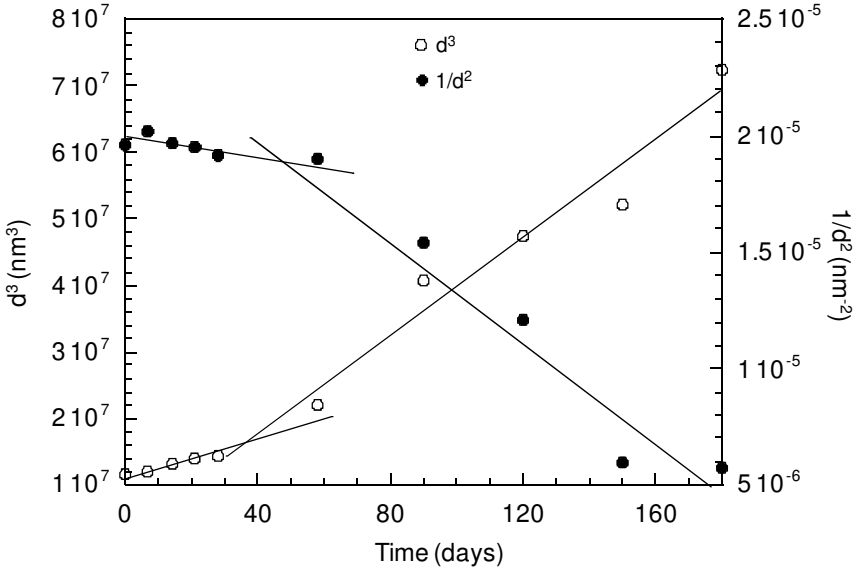
8 10^7
7 10^7
6 10^7
5 10^7
4 10^7
3 10^7
2 10^7
1 10^7
d^3 (nm^3)
2.5 10^-5
2 10^-5
1.5 10^-5
1 10^-5
5 10^-6
1/d^2 (nm^-2)
d^3
1/d^2
0
40
80
120
160
Time (days)

Figure 6

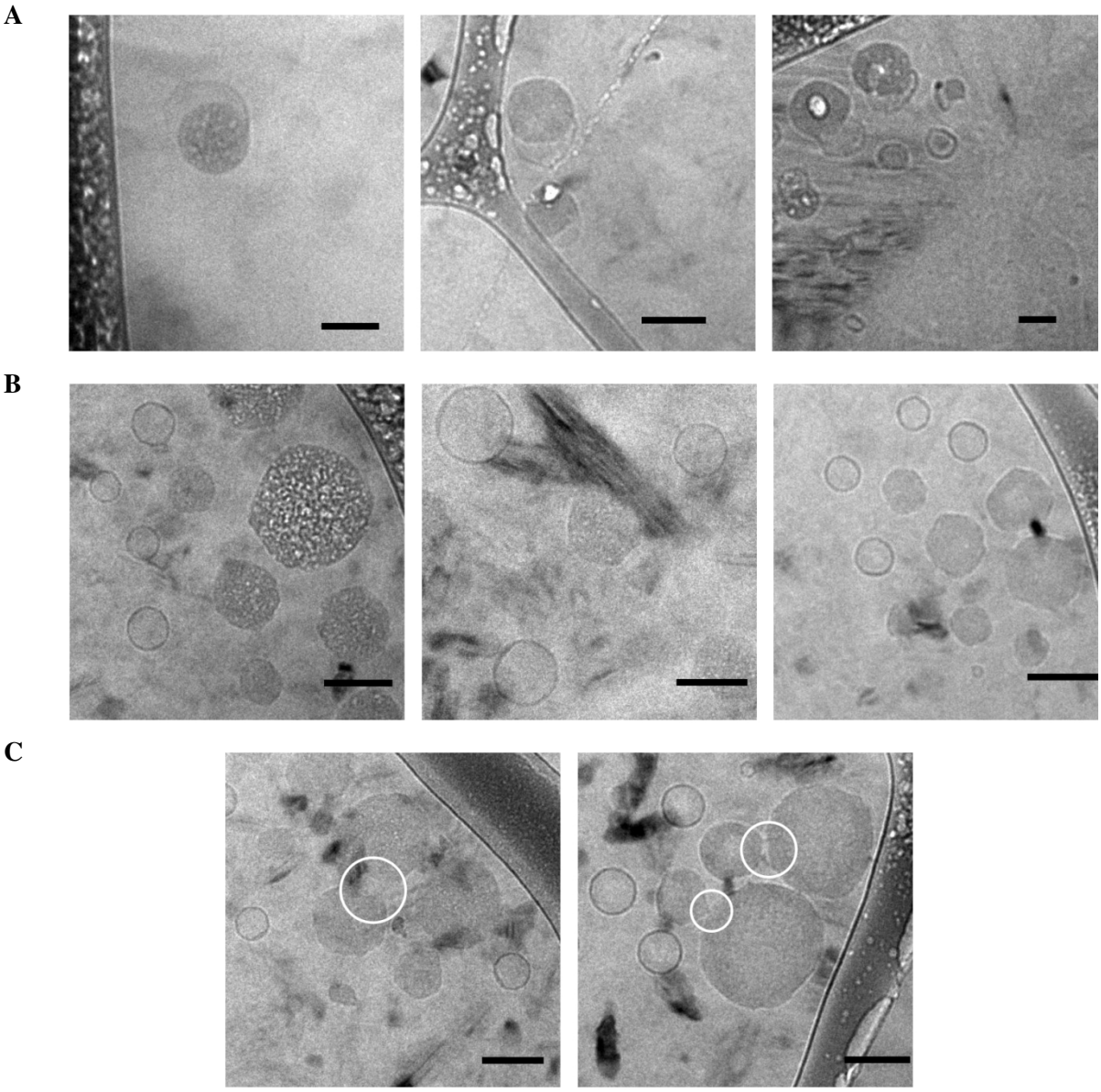

Figure 7

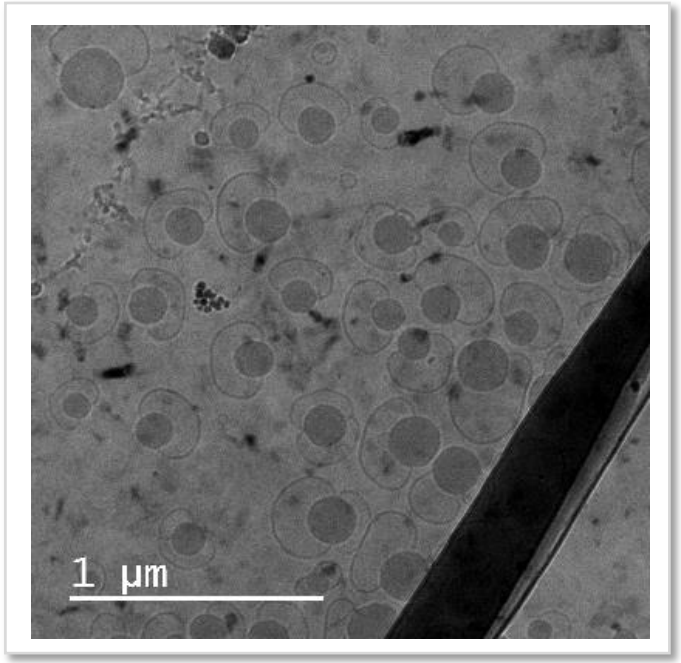
1 µm

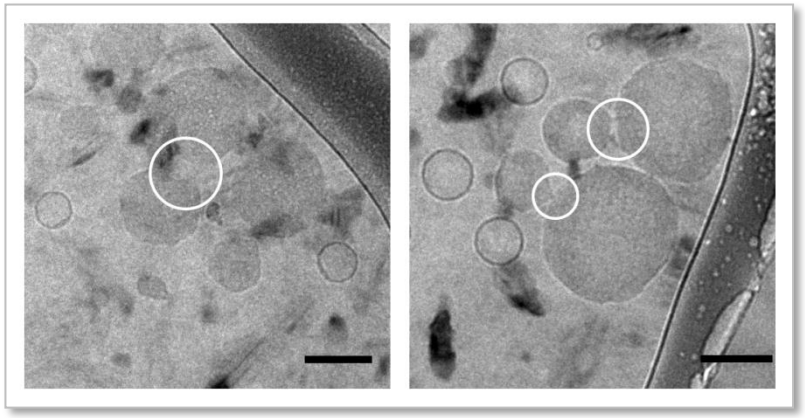

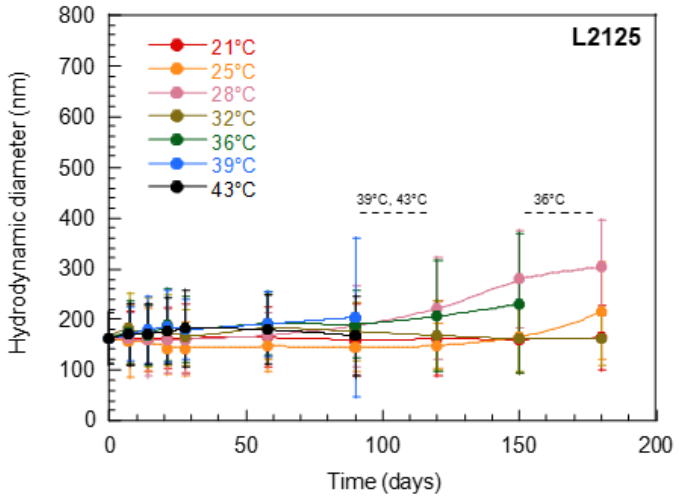
L2125
21°C
25°C
28°C
32°C
36°C
39°C
43°C
39°C, 43°C
36°C
Hydrodynamic diameter (nm)
Time (days)

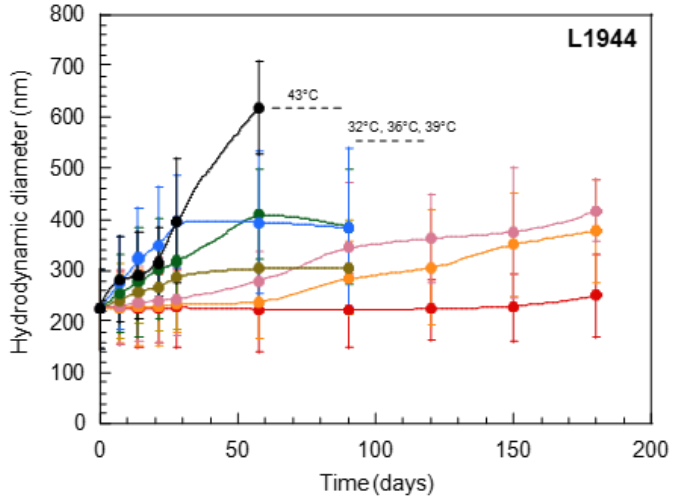
L1944
43°C
32°C, 36°C, 39°C
Hydrodynamic diameter (nm)
Time (days)

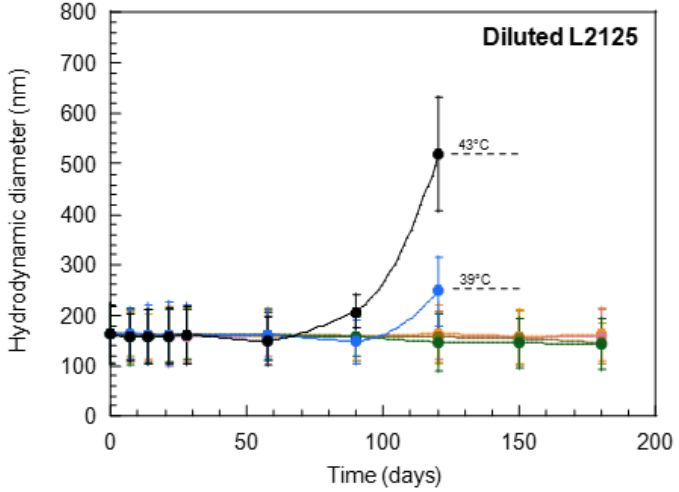
Diluted L2125
43°C
39°C
Hydrodynamic diameter (nm)
Time (days)

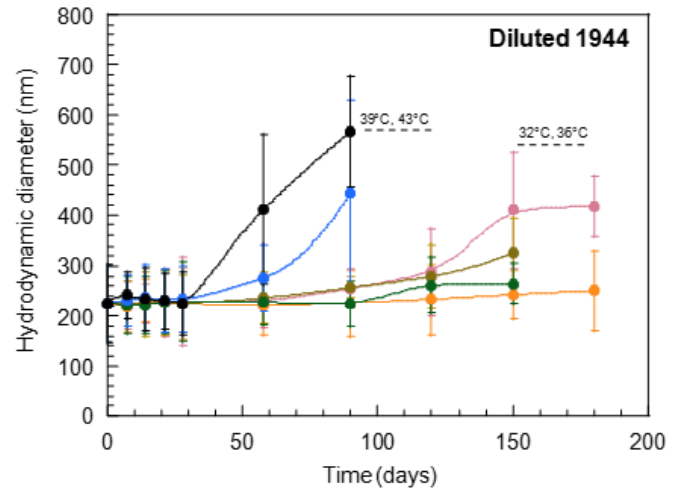
Diluted 1944
39°C, 43°C
32°C, 36°C
Hydrodynamic diameter (nm)
Time (days)